Lawrence Berkeley National Laboratory

Title

High Areal Capacity Si/LiCoO2 Batteries from Electrospun Composite Fiber Mats

Permalink

https://escholarship.org/uc/item/8px6n0sh

Journal

ChemSusChem, 10(8)

ISSN

1864-5631

Authors

Self, Ethan C
Naguib, Michael
Ruther, Rose E
et al.

Publication Date

2017-04-22

DOI

10.1002/cssc.201700096

Peer reviewed

High Areal Capacity Si/LiCoO$_2$ Batteries from Electrospun Composite Fiber Mats

Ethan C. Self,[a] Michael Naguib,[b] Rose E. Ruther,[b] Emily C. McRen,[a] Ryszard Wycisk,[a] Gao Liu,[c] Jagjit Nanda,[b] and Peter N. Pintauro*[a]

Freestanding nanofiber mat Li–ion battery anodes containing Si nanoparticles, carbon black, and poly(acrylic acid) (Si/C/PAA) are prepared using electrospinning. The mats are compacted to a high fiber volume fraction (≈ 0.85), and interfiber contacts are welded by exposing the mat to methanol vapor. A compacted+welded fiber mat anode containing 40 wt% Si exhibits high capacities of 1484 mA h g^{-1} (3500 mA h g$_{Si}^{-1}$) at 0.1 C and 489 mA h g^{-1} at 1 C and good cycling stability (e.g., 73% capacity retention over 50 cycles). Post-mortem analysis of the fiber mats shows that the overall electrode structure is preserved during cycling. Whereas many nanostructured Si anodes are hindered by their low active material loadings and densities, thick, densely packed Si/C/PAA fiber mat anodes reported here have high areal and volumetric capacities (e.g., 4.5 mA h cm^{-2} and 750 mA h cm^{-3}, respectively). A full cell containing an electrospun Si/C/PAA anode and electrospun LiCoO$_2$-based cathode has a high specific energy density of 270 Wh kg^{-1}. The excellent performance of the electrospun Si/C/PAA fiber mat anodes is attributed to the: i) PAA binder, which interacts with the SiO$_x$ surface of Si nanoparticles and ii) high material loading, high fiber volume fraction, and welded interfiber contacts of the electrospun mats.

Introduction

Since their commercial debut in 1991, Li–ion batteries (LIBs) have revolutionized the functionality of portable electronic devices, and the LIB industry continues to grow today owing to emerging applications such as electric vehicle propulsion.[1,2] Despite the extraordinary success of LIBs, many devices are still limited by battery performance, and thus new batteries with higher energy densities and long cycle life must be developed to satisfy the ever-increasing demands of consumers.[3–5]

Si has been widely investigated as a replacement for graphite in today's LIB anodes owing to its high theoretical capacity (3600 mA h g^{-1} for Li$_{15}$Si$_4$ vs. 372 mA h g^{-1} for LiC$_6$) and low operating potential (<0.5 V vs. Li/Li$^+$).[6–7] However, Si-based anodes often exhibit poor cycling stability due to a number of issues, primarily the large volume changes during cycling and instabilities associated with the solid–electrolyte interphase (SEI) layer. Lithiation of Si is accompanied by a volumetric expansion exceeding 300%, and repeated swelling and shrinking of Si during battery cycling results in capacity fade due to Si pulverization, electronic isolation of Si particles, and irreversible Li consumption associated with repeated formation and rupture of the SEI layer.[8–11] Although Si pulverization can be eliminated through the use of nanoscale active materials (e.g., Si nanoparticles[12–14] and Si nanowires)[15–18] and/or new electrode architectures, effective techniques that prevent electronic isolation of Si and stabilize the SEI layer are yet to be identified.[8,9] Furthermore, previously reported nanoscale Si anodes typically contained low active material loadings and densities, resulting in low areal and volumetric capacities. To produce Si anodes that are suitable for commercial applications, new anode designs that can tolerate Si volumetric changes while maintaining high gravimetric, areal, and volumetric capacities over many charge/discharge cycles must be developed.

Fiber structures have been receiving increased attention recently as battery electrodes.[19–37] For electrospun Si anodes, previous studies utilized pyrolyzed fibers with embedded Si particles to create an electronically conductive Si/C nanofiber network.[27–36] Freestanding Si/C nanofiber mats exhibited high gravimetric capacities (e.g., 800–1600 mA h g^{-1}) and good stability over 30–100 cycles, but most of these studies neglected to carefully examine the anode's areal and volumetric capacities. Si areal loadings in many electrospinning studies were very low (e.g., <0.1 mg$_{Si}$ cm^{-2}),[33,38] and SEM images suggest that the fiber volume fractions of the mats were far too low (<0.25) for practical battery applications.

An alternative to pyrolyzed carbon-fiber-based electrodes is the use of electrospun particle/polymer fiber mat electrodes, an approach that has been pursued by Pintauro and co-

[a] Dr. E. C. Self, E. C. McRen, Prof. R. Wycisk, Prof. P. N. Pintauro
Department of Chemical and Biomolecular Engineering
Vanderbilt University
Nashville, TN 37235 (USA)
E-mail: pn.pintauro@vanderbilt.edu

[b] Dr. M. Naguib, Dr. R. E. Ruther, Dr. J. Nanda
Materials Science and Technology Division
Oak Ridge National Laboratory
Oak Ridge, TN 37831 (USA)

[c] Dr. G. Liu
Energy Storage and Distributed Resources Division
Lawrence Berkeley National Laboratory
Berkeley, CA 94720 (USA)

workers.[19–21] The preparation and characterization of several particle/polymer fiber mat LIB electrodes have been reported, including: i) anodes containing titania nanoparticles, carbon powder, and poly(acrylic acid) (TiO$_2$/C/PAA);[19] ii) anodes containing carbon powder and poly(vinylidene fluoride) (C/PVDF);[20] and iii) cathodes containing LiCoO$_2$ nanoparticles, carbon powder, and PVDF (LiCoO$_2$/C/PVDF).[21] These studies showed that fiber mats with a high material loading (e.g., 54.1 mg cm^{-2}) and high fiber volume fractions (up to 0.86) worked exceptionally well, with high areal and volumetric capacities at fast charge/discharge rates (e.g., 1.3 mA h cm^{-2} and 62 mA h cm^{-3} at 2 C). The excellent performance of electrospun particle/polymer fiber mat electrodes is attributed to: i) a large electrode–electrolyte interfacial area, ii) short Li$^+$ transport pathways between the electrolyte and active material in the radial fiber direction, and iii) good electrolyte infiltration throughout the electrode through the intra- and interfiber void space of the mat.

Based on our encouraging prior results with electrospun particle/polymer electrodes containing moderate capacity materials,[19–21] it makes sense to apply the technique to high capacity Si-based anodes. A particle/polymer fiber mat containing Si nanoparticles is fundamentally different from and offers several advantages over previously reported Si/C fiber anodes prepared by high-temperature pyrolysis. The presence of the polymer binder ensures that particle/polymer fiber mats can be compacted under high pressure without fracturing, and thus thick, densely packed nanofiber electrodes can be created for high gravimetric, areal, and volumetric capacities.[19–21] High areal capacity is desired to reduce the relative amount of inactive cell components (e.g., current collectors and separators), and high volumetric capacity is critical for many applications in which the space allotted for a battery is limited (e.g., electric vehicles).[7, 19–21] Electrospun particle/polymer fibers can also be made with a binder that absorbs electrolyte, ensuring that Li$^+$ ions have access to most/all Si nanoparticles in the electrode. Furthermore, the binder in such fiber mats can be chosen to accommodate the volume changes of Si particles during charge/discharge cycling, as has been reported for electronically conductive binders[39–42] and binders like PAA,[43] carboxymethyl cellulose,[44] and alginate,[45] which form hydrogen bonds with the SiO$_x$ layer on Si. Preserving the binder in the electrode structure also allows interfiber crossings to be welded by exposure to solvent vapor. A welded fiber mat is expected to have improved mechanical properties and thus better cycling stability compared to an unwelded electrospun mat. These advantages are unique to a particle/polymer system and cannot be realized for Si/C fibers prepared by high-temperature pyrolysis. Finally, freestanding particle/polymer nanofiber mats can be used directly as LIB electrodes and do not require metal foil current collectors, allowing for higher cell-level energy densities.[46]

The results reported here point to significant advances in which electrospinning is used to develop composite fiber mat LIB electrodes containing Si nanoparticles, carbon powder, and PAA (Si/C/PAA). The first part of this study demonstrates that Si/C/PAA fiber mats have high gravimetric capacities of 1484 mAh g^{-1} at 0.1 C and 489 mA h g^{-1} at 1 C and good cycling stability over 50 cycles. Thick, highly compacted fiber mats are used to achieve high areal and volumetric capacities of 4.5 mA h cm^{-2}, and 750 mA h cm^{-3}, respectively. Qualitative performance–composition–structure correlations are established by evaluating the performance of freestanding fiber mats with different compositions, fiber volume fractions, interfiber connectivities, thicknesses, and loadings. The electrospinning approach is also used with a LiCoO$_2$-cathode chemistry to develop the first Si/LiCoO$_2$ battery containing an electrospun anode and electrospun cathode. Electrospun fiber mat electrodes are commercially scalable and can be intergrated into a roll-to-roll platform. This study opens new opportunities to utilize electrospun LIBs for other functional energy storage devices such as structural batteries, wearables, and stationary applications.[47]

Results and Discussion

Freestanding fiber mats containing Si nanoparticles, carbon powder, and a PAA binder (Si/C/PAA) were fabricated using electrospinning. Preparing particle/polymer fiber mats with a uniform particle distribution requires optimization of several experimental parameters (e.g., ink composition, flow rate, electric field strength, etc.), and thus appropriate ink formulation and electrospinning conditions were determined empirically rather than through a priori means. An example of a non-optimized fiber mat structure that contains large particle aggregates (> 5 μm in diameter) is shown in Figure S1 in the Supporting Information. Herein, n-propanol was used as the solvent in all inks, and fiber mats containing Si/C/PAA in a weight ratio of 40/25/35 were produced using a fixed ink flow rate of 1.00 mL h^{-1}, applied bias voltage of 8 kV, and a spinneret-to-collector distance of 8 cm, as these conditions were used in our previous report on TiO$_2$-based fiber mat anodes.[19] Ink formulation and relative humidity during electrospinning were then optimized to form Si/C/PAA fiber mats. The solids content of the inks (i.e., combined amounts of Si nanoparticles, carbon powder, and PAA) was varied from 10–30 wt %, and 17–18 wt % solids was found to be optimal. Inks containing > 25 wt % solids could not be dispersed using magnetic stirring and sonication, and inks with 10–15 wt % solids had low viscosities that were not appropriate for electrospinning. Relative humidity (rh) during electrospinning had a significant impact on the properties of the fiber mats. Electrospinning at > 30 % rh resulted in the deposition of fibers that could not be peeled from the collector, presumably owing to incomplete solvent evaporation of the fiber jet. On the other hand, freestanding fiber mats were produced by electrospinning at 20–30 % rh, and thus these conditions were used herein.

Scanning electron microscopy (SEM) images of an electrospun nanofiber mat containing Si/C/PAA in a 40/25/35 weight ratio are shown in Figure 1. The as-spun mat had a fiber volume fraction of 0.30 and an average fiber diameter of 980 nm with some bead-on-fiber formation (see Figure 1 a, b); these observations were typical for fiber mats prepared in this
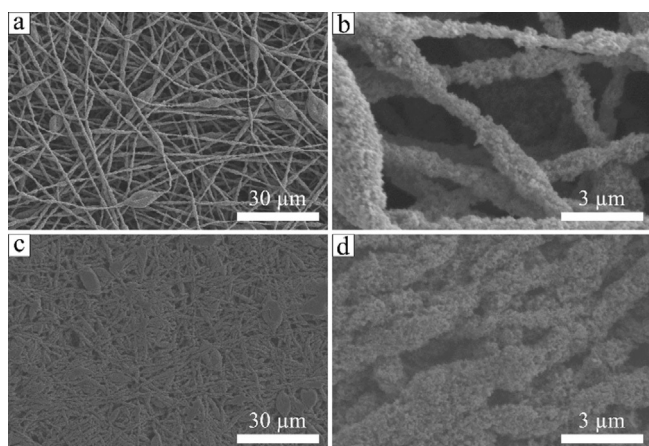
Figure 1. Top-down SEM images of electrospun nanofiber mats containing Si/C/PAA in a 40/25/35 weight ratio: a, b) an as-spun fiber mat and c, d) a compacted + welded fiber mat.

study. Compacting the mat increased the fiber volume fraction to 0.85, whereas welding the mat improved the interfiber connectivity. As shown in Figure 1 c, d, a mat that was both compacted and welded (from hereon referred to as a compacted + welded fiber mat) maintained some interfiber void space, and corresponding cross-sectional the SEM images presented in Figure 2 a, b demonstrate that the fiber volume fraction was
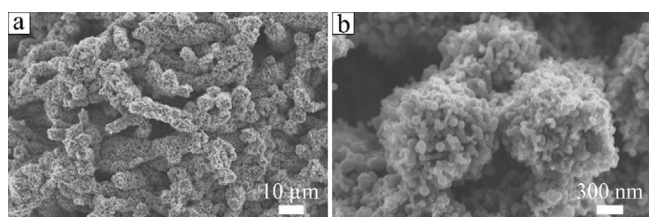

Figure 2. a) Low and b) high magnification cross-sectional SEM images of a compacted + welded fiber mat containing Si/C/PAA in a 40/25/35 weight ratio.

uniform throughout the mat and that the interfiber contact nodes were successfully welded. Compared to the as-spun mat, the compacted + welded mat was mechanically stiffer, confirming the presence of these fused fiber crossings. The interfiber connectivity was also assessed by measuring the electrical resistance over a 2 cm section of mat using an ohmmeter with point-type probes. The measured resistance of a compacted + welded mat was ≈1000 times lower than that of an as-spun mat (4 vs. 3000 kΩ), indicating the compacted + welded fiber mat had much better interfiber connectivity.

An X-ray diffraction (XRD) pattern of an as-spun Si/C/PAA fiber mat is shown in Figure S2. Peaks associated with crystalline Si were observed in good agreement with the JCPDS powder diffraction file (PDF No. 27-1402). The broad peaks near $2\theta = 20°$ are attributed to the carbon powder and PAA binder.[48] An energy-dispersive X-ray spectroscopy (EDX) analysis of a Si/C/PAA fiber mat (see Figure S3) demonstrates that Si and C were evenly distributed throughout the fiber structure,

which is consistent with the SEM images shown in Figures 1 and 2.

The performance of an as-spun nanofiber mat anode with a Si/C/PAA weight ratio of 40/25/35 was compared to that of a compacted + welded mat of the same composition. Figure 3 a shows charge/discharge curves collected at 0.1 C for
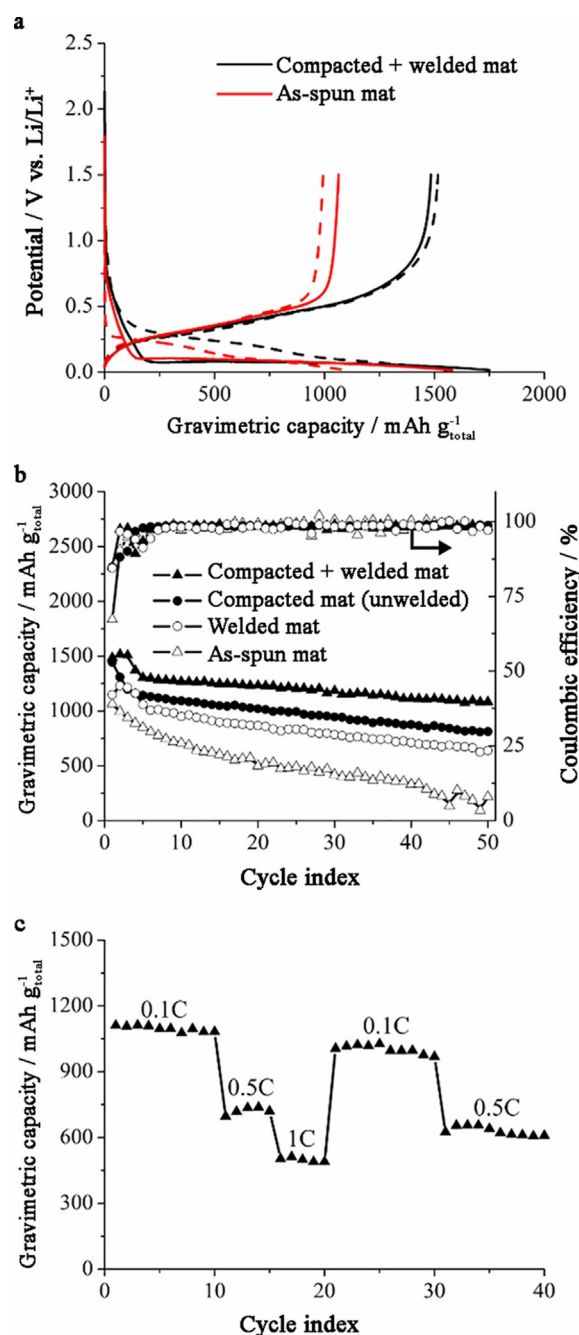

Figure 3. Electrochemical characterization of electrospun anodes containing Si/C/PAA in a 40/25/35 weight ratio: a) charge/discharge curves for the 1st and 2nd cycles (solid and dashed lines, respectively) for as-spun and compacted + welded fiber mats, b) gravimetric capacity over 50 cycles at 0.1 C for as-spun, compacted (unwelded), welded (uncompacted), and compacted + welded fiber mats, and c) gravimetric capacity of a compacted + welded fiber mat at 0.1–1 C. Gravimetric capacities are normalized with respect to the overall mass of the fiber mat anodes. The electrode loading was ≈0.7 mg cm^{-2} for all samples.

each electrode during the first two cycles. The shapes of these curves are typical for Si-based anodes in which lithiation and delithiation reactions occur at potentials <0.5 V versus Li/Li$^+$.[6] Both electrodes exhibited high lithiation capacities ≈ 1700 mAh g^{-1} during the first cycle, but the as-spun mat had a low reversible capacity of 1064 mAh g^{-1} (corresponding to ≈ 2500 mAh g$_{Si}^{-1}$ and 67% coulombic efficiency), suggesting some fibers in the as-spun mat were electronically isolated during the first delithiation half cycle. In comparison, the compacted + welded fiber mat anode had excellent Si utilization as evidenced by a high reversible capacity of 1484 mAh g^{-1} (corresponding to ≈ 3500 mAh g$_{Si}^{-1}$ and 85% coulombic efficiency), which was essentially unchanged during the second charge/discharge cycle.

Figure 3b shows the gravimetric capacity over 50 cycles at 0.1 C of four electrospun anodes with a Si/C/PAA weight ratio of 40/25/35, including: i) an as-spun mat, ii) a compacted (unwelded) mat, iii) a welded (uncompacted) mat, and iv) a compacted + welded mat. The fiber volume fractions of the uncompacted and compacted mats were approximately 0.30 and 0.85, respectively. The as-spun mat had the lowest initial capacity of 1064 mAh g^{-1}, which faded steadily to 218 mAh g^{-1} after 50 cycles. In comparison, the compacted + welded fiber mat anode showed reasonably good cycling performance with reversible capacities of 1484 and 1083 mAh g^{-1} during the 1st and 50th cycles, respectively. Mats that were only welded or only compacted showed intermediate cycling performance. These results demonstrate that mats with a fiber volume fraction of 0.85 and welded interfiber contacts have sufficient void space for electrolyte infiltration throughout the electrode and mechanical strength to withstand the large volumetric changes of Si during cycling. Conversely, mats with a low fiber volume fraction (≈ 0.30) and/or poor interfiber connectivity cannot tolerate reversible Si swelling/shrinking.

The gravimetric capacity of a compacted + welded Si/C/PAA fiber mat anode (prepared with 40 wt% Si, a fiber volume fraction of 0.85, and a thickness of 22 μm) at charge/discharge rates of 0.1–1 C over 40 cycles is shown in Figure 3c. This rate capability study was conducted after stabilizing the electrode for 40 cycles at 0.1 C at which point the reversible capacity was 1113 mAh g^{-1}. Overall, the Si/C/PAA fiber mat had good rate capabilities with stable capacities of 722 and 489 mAh g^{-1} at 0.5 C and 1 C, respectively. The capacity at 0.1 C was fully recovered after cycling at 1 C. The good performance of the electrospun fiber mat anode at high C-rates is attributed to rapid Li$^+$ transport between the electrolyte and Si nanoparticles in the radial fiber direction, which is a consequence of the small fiber diameter (≈ 1 μm) and electrolyte penetration throughout the mat's interfiber void space. These results are consistent with our previous reports on other electrospun particle/polymer fiber mat electrodes for Li–ion batteries.[19–21]

Thick electrodes with high areal capacities are desired to reduce the relative amount of inactive components (e.g., current collectors, separators, etc.) in a Li–ion battery. To determine how electrode loading and thickness affect areal capacity and cycling stability, compacted + welded fiber mat anodes (Si/C/PAA weight ratio of 40/25/35) at two different loadings

(0.71 and 3.49 mg cm^{-2} with thicknesses of 22 and 65 μm, respectively) were characterized over 50 cycles at 0.1 C. The thin electrode was prepared from a single layer of an electrospun mat that was compacted and welded, whereas the thick electrode with higher loading was prepared by stacking 5 individual mats followed by the compaction and welding steps. The measured densities of the thin and thick electrodes were 0.32 and 0.54 g cm^{-3}, corresponding to porosities of 82 and 70%, respectively; these porosities were sufficient for good electrolyte infiltration throughout the fiber mats. As shown in Figure 4a, the initial gravimetric capacity was essentially the same for the two mats when normalized to the total electrode mass (1300 mAh g^{-1} at 3.49 mg cm^{-2} and 1484 mAh g^{-1} at 0.71 mg cm^{-2}), and each anode retained $\approx 70\%$ of its initial capacity after 50 cycles. As expected, the primary difference in the two nanofiber anodes was their areal capacities (see Figure 4b). Notably, the thick anode (with a loading of 3.49 mg cm^{-2}) exhibited very high areal and volumetric capacities of 4.5 mAh cm^{-2} and 750 mAh cm^{-3}, which exceed that of commercial graphite anodes (e.g., ≈ 3 mAh cm^{-2} and 350 mAh cm^{-3} at 0.2 C for an anode with a loading of 7.9 mg$_{graphite}$ cm^{-2}).[49] Furthermore, as the electrospun fiber mats do not require a metal foil current collector, they can be
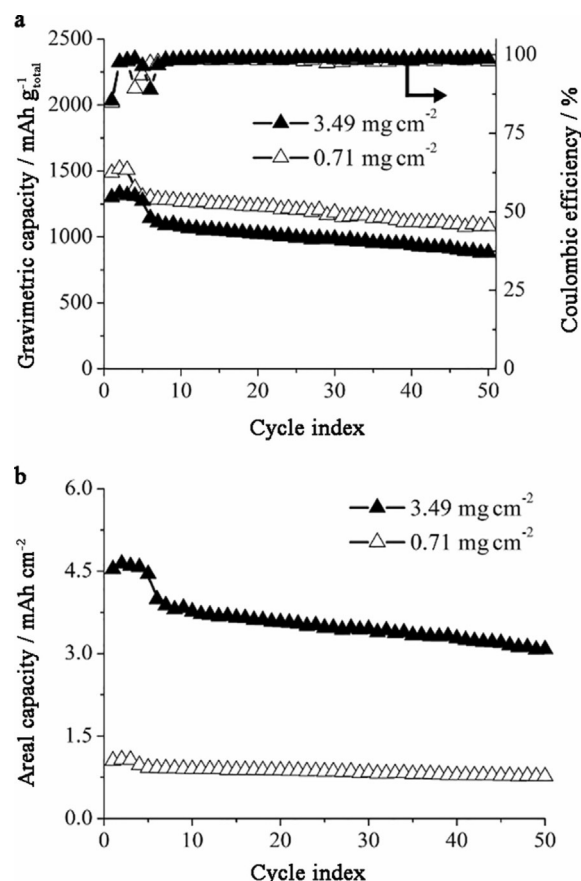

Figure 4. a) Gravimetric capacity and b) areal capacity of compacted + welded Si/C/PAA nanofiber mats over 50 cycles at 0.1 C. Electrodes at two different loadings (0.71 and 3.49 mg cm^{-2}) were characterized. The electrodes contained Si/C/PAA in a 40/25/35 weight ratio. Gravimetric capacities are normalized with respect to the overall mass of the fiber mat anodes.

used to prepare a Li–ion battery with significantly increased specific energy density compared to today's state-of-the-art batteries. In commercial graphite anodes, the current collector accounts for approximately half of the electrode mass, and the anode (including current collector) accounts for 25% of the battery weight.[50] Thus, it is expected that a freestanding compacted+welded Si/C/PAA fiber mat anode could reduce battery weight by $\approx$25% (or equivalently, increase the specific energy density by $\approx$25%). Overall, the excellent performance of the particle/polymer fiber mat anodes is attributed to the good binder/particle adhesion (i.e., PAA interacts with the SiO_x surface on Si nanoparticles through hydrogen bonding),[43] the high Si loading in the fibers, a sufficient (but not excessive) interfiber porosity for electrolyte infiltration, and the presence of interfiber welds (where both welding and a high fiber volume fraction impart mechanical strength to the mat).

The performance of the compacted+welded Si/C/PAA fiber mat anodes in Figure 4 compare well to electrospun Si-based anodes reported in the literature. Xiao et al.[38] prepared and characterized a coaxial electrospun nanofiber mat prepared by sputtering a Si layer onto Ni-plated PVDF nanofibers. The electrode exhibited a high capacity when normalized to the Si active material (3210 mA h g_{Si}^{-1}), but the Si loading in the fibers was only 18.1 wt%, corresponding to an effective gravimetric capacity of 581 mA h g^{-1}. Furthermore, this electrode had a very low material loading of 0.08 mg cm^{-2}, with an areal capacity of 0.046 mA h cm^{-2}, which is far too low for practical battery applications. In another study, Xu et al.[31] prepared a 3D Si/C fiber anode by electrospinning poly(acrylonitrile) fibers and electrospraying Si nanoparticles, followed by high-temperature pyrolysis to create an electronically conductive nanofiber network. The electrode exhibited stable performance over 100 cycles with high gravimetric and volumetric capacities (1600 mA h g^{-1} and 1000 mAh cm^{-3}, respectively), but the areal capacity (2.7 mA h cm^{-2}) was lower than that of the Si/C/PAA fiber mat anodes reported here (4.5 mAh cm^{-2}).

In principle, the thickness of electrospun Si/C/PAA anodes can be further increased to achieve even higher areal capacities than those reported in Figure 4. Our previous studies[19–21] on electrospun particle/polymer fiber mat electrodes demonstrated that fiber mats that are several hundred microns thick have good active material utilization at slow and fast charge/discharge rates. Extrapolating the results shown in Figure 4, a 200 μm thick Si/C/PAA fiber mat with a fiber volume fraction $\approx$0.80 would have an extremely high areal capacity of 14 mA h cm^{-2} at 0.1 C, which is an order of magnitude greater than that of state-of-the-art materials. Although such electrodes were not prepared in this study, these experiments are currently underway, and the effect of Si/C/PAA fiber mat thickness and porosity on electrode capacity and rate capabilities will be the subject of a future publication.

To determine how the structure of the electrospun Si/C/PAA anodes evolved during charge/discharge cycling, post-mortem analyses of a fiber mat electrode containing 40 wt% Si were conducted. Figure 5 shows Raman spectra for a pristine (i.e., uncycled) fiber mat anode and an electrode after 50 cycles at 0.1 C. The pristine electrode had a large peak near 520 cm^{-1},
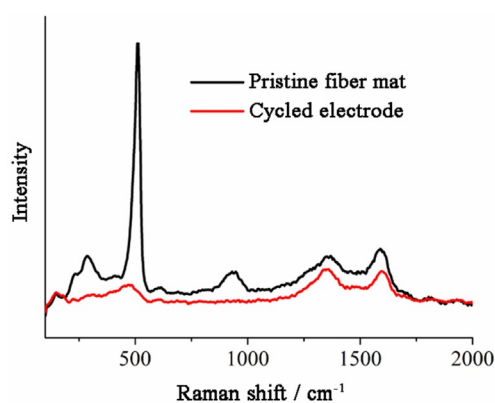
Figure 5. Raman spectra of Si/C/PAA fiber mat anodes before and after 50 cycles at 0.1 C. The electrodes contained Si/C/PAA in a 40/25/35 weight ratio.

associated with the presence of crystalline Si.[51–53] This peak was absent in the cycled electrode, which contained a broad peak near 475 cm^{-1}, indicating a crystalline to amorphous transformation of Si during cycling.[52,54] This change was mapped over a large area $\approx$4.5×9.0 μm^2 as shown in Figure 6;

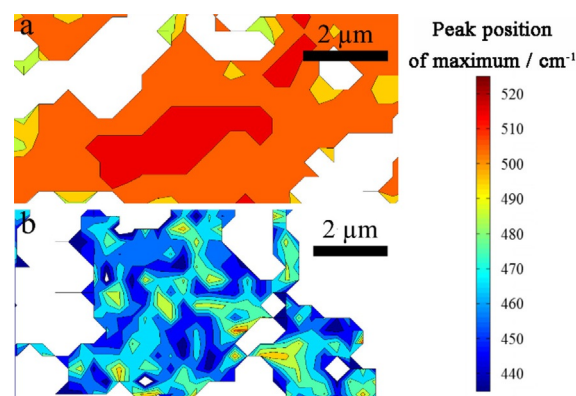**Figure 6.** Raman maps over an area of $\approx$4.5×9.0 μm^2 showing the Raman shift of the maximum peak for Si/C/PAA fiber mat anodes: a) before cycling and b) after 50 cycles at 0.1 C. White pixels represent regions where the data were omitted owing to low spectral intensities (i.e., counts <10). The electrodes contained Si/C/PAA in a 40/25/35 weight ratio.

these results indicate that the transformation occurred uniformly throughout the fiber mat. Compared to crystalline Si, the peaks for amorphous silicon were broader and weaker, which resulted in some spatial variation in the peak positions for the cycled electrode. Note that portions of the electrode surfaces were out of focus during Raman mapping, and the white pixels in Figure 6 represent regions where the data were omitted owing to low spectral intensities (i.e., counts <10).

SEM images of Si/C/PAA fiber mat cross-sections taken before and after 50 charge/discharge cycles are shown in Figure 7. These images reveal features related to the: i) overall electrode structure (Figure 7 a, b), ii) interfiber void space (Figure 7 c, d), and iii) individual particle structure (Figure 7 e, f). There was a small (11%) increase in electrode thickness, from
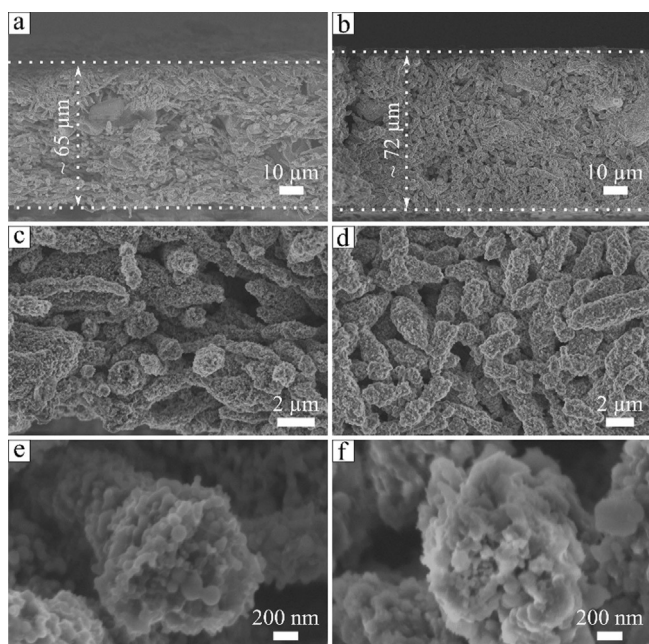
Figure 7. Cross-sectional SEM images of a Si/C/PAA nanofiber mat anode: a, c, e) before cycling and b, d, f) after 50 cycles at 0.1 C. The electrodes contained Si/C/PAA in a 40/25/35 weight ratio.
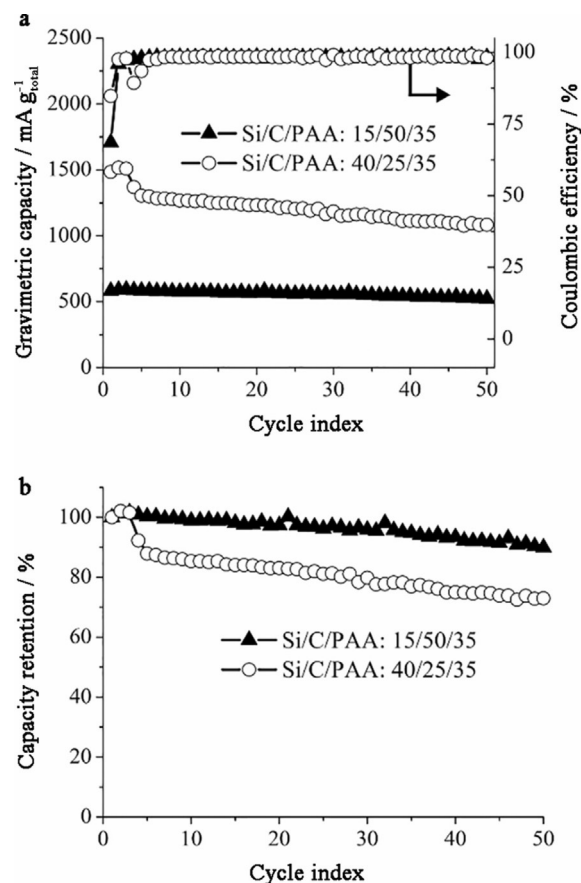

Figure 8. Electrochemical characterization of compacted + welded nanofiber mat anodes containing Si/C/PAA weight ratios of 40/25/35 and 15/50/35: a) gravimetric capacity and b) capacity retention over 50 cycles at 0.1 C. Gravimetric capacities are normalized with respect to the overall mass of the fiber mat anodes. All electrodes were prepared with ≈ 0.26 mg$_{Si}$ cm^{-2}.

65 to 72 μm before/after cycling, as indicated by the low magnification images in Figure 7 a, b. In comparison, Piper et al.[55] found that the thickness of a slurry cast anode containing Si nanoparticles, carbon black, and PVDF increased by 50 % after 20 cycles. Thus, there is visual evidence that the nanofiber mat anode was able to reversibly accommodate the volumetric expansion/contraction of Si with minimal changes to the overall electrode structure. As presented in Figure 7 c, d, the interfiber void space throughout the mat was also well-preserved during cycling. The high magnification image of a single fiber in Figure 7 e shows spherical Si particles before cycling, whereas the cycled fiber (Figure 7 f) contained irregularly shaped particles. This change in particle appearance is attributed to the formation of an SEI layer on the fiber surface that masked the particle shape and/or actual changes in particle morphology during cycling owing to the formation of amorphous Si. Overall, these post-mortem SEM images demonstrate that the fiber mat anodes exhibited excellent physical stability during charge/discharge cycling in a battery environment.

As a final half-cell experiment, the effect of Si content in the fibers on cycling performance was evaluated. A compacted + welded mat with a Si/C/PAA fiber weight ratio of 15/50/35 and a fiber volume fraction of 0.85 was prepared (see Figure S4), and the performance of this anode was compared to that of a compacted + welded mat in which the fibers contained 40 wt % Si. The areal loading of Si in both anodes was fixed at ≈ 0.26 mg$_{Si}$ cm^{-2}, which translates to a theoretical areal capacity of ≈ 1 mA h cm^{-2}. To achieve this areal capacity match, the mat with 15 wt % Si was made thicker (40 μm vs. 22 μm for the anode with 40 wt % Si). As shown in Figure 8 a, the anode with 15 wt % Si had a lower effective gravimetric capacity (582 vs. 1484 mA h g^{-1}) owing to the lower Si content in the fibers, but

both electrodes exhibited good Si utilization with reversible capacities > 3000 mA h g$_{Si}^{-1}$. Figure 8 b shows that the anode with lower Si content displayed excellent cycling stability with 90 % capacity retention after 50 cycles versus 73 % capacity retention for the anode containing 40 wt % Si. The better cycling stability of the 15 wt % Si anode is attributed to smaller net volume changes of the fibers during charging and discharging. Overall, these results demonstrate that the lower effective gravimetric capacity of the anode containing 15 wt % Si can be offset by increasing the electrode thickness to achieve the same areal capacity as a fiber mat with a higher Si weight fraction.

Most of the existing literature on Si-based anodes focuses exclusively on half-cell characterizations, but electrode performance in full cells is critical for practical battery applications.[7,9,21] To evaluate electrode performance under more practical testing conditions, a full cell containing an electrospun Si/C/PAA anode (with a Si/C/PAA weight ratio of 40/25/35) and an electrospun LiCoO$_2$/C/PVDF cathode[21] was prepared and characterized.

Figure 9 a shows a typical charge/discharge curve at 0.1 C for the electrospun Si/LiCoO$_2$ full cell. During discharge, the cell had an average operating potential of 3.6 V and a reversible
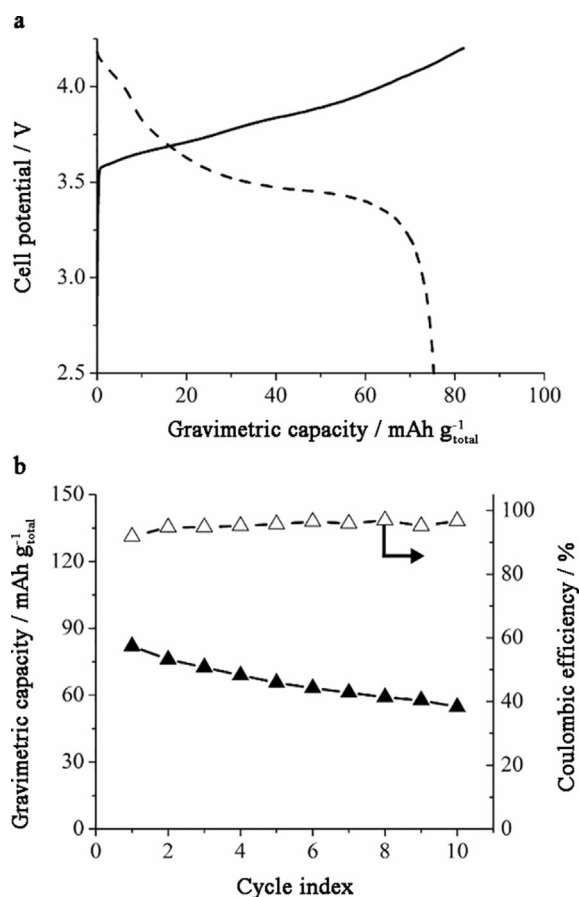
Figure 9. Electrochemical characterization of a full cell containing an electrospun Si/C/PAA anode and LiCoO$_2$/C/PVDF cathode: a) charge/discharge curve collected during the first cycle at 0.1 C and b) cycling stability over 10 cycles at 0.1 C. The anode contained Si/C/PAA in a 40/25/35 weight ratio, and the cathode contained LiCoO$_2$/C/PVDF in a 70/10/20 weight ratio. Gravimetric capacities are normalized with respect to the combined mass of the fiber mat anode and cathode.

capacity of 75 mA h g^{-1} (normalized to the combined mass of both electrodes), which corresponds well to the theoretical capacity of 77 mA h g^{-1} based on the individual capacities of the anode and cathode. Agreement between the measured and theoretical capacities indicates good active material utilization for the Si-based anode and LiCoO$_2$-based cathode. The areal capacity and energy density of the Si/LiCoO$_2$ cell were 2.6 mA h cm^{-2} and 270 W h kg^{-1}, respectively, which are the highest values reported to date in the literature for any electrospun full cell (previous studies reported effective areal capacities < 1 mA h cm^{-2} and mass normalized specific energies of 100–150 W h kg^{-1}).[56–57] Figure 9b shows the Si/LiCoO$_2$ full cell exhibited moderate cycling stability with a reversible capacity of 53 mA h g^{-1} after 10 cycles. Compared to half-cell experiments, which showed stable performance of the anode and cathode, the moderate capacity fading of the full cell is attributed to irreversible Li losses between charging and discharging steps. The cycling stability may be improved by placing excess Li reserves in the cell (e.g., by decreasing the N/P ratio), and these experiments will be the subject of a future study. Overall, this work demonstrates promising proof-of-concept for a full cell containing a freestanding anode and

cathode prepared by particle/polymer electrospinning. Furthermore, it should be noted that the energy density of the Si/LiCoO$_2$ cell was limited by the cathode capacity (84 mA h g^{-1} at 0.1 C); thus the use of a higher capacity cathode material (e.g., sulfur) would lead to even higher full cell energy densities.

Conclusions

Particle/polymer electrospinning was used to prepare fiber mat Li–ion battery anodes containing Si nanoparticles and carbon black with poly(acrylic acid) as the binder (Si/C/PAA). Compacting and welding improved the mechanical strength of an electrospun mat, but sufficient void space remained in the electrode to accommodate the large volumetric changes of Si during charge/discharge cycling. A compacted + welded fiber mat containing 40 wt % Si had a high gravimetric capacity of 1484 mA h g^{-1} (3500 mA h g$_{Si}^{-1}$) and good cycling stability with 73 % capacity retention after 50 cycles at 0.1 C. The effect of Si content in the fibers on cycling performance was also evaluated. Compared to an anode prepared with 40 wt % Si, a fiber mat containing 15 wt % Si had a lower effective gravimetric capacity (582 mA h g^{-1}) but better cycling stability (e.g., 90 % capacity retention after 50 cycles) owing to smaller overall volumetric changes during cycling. The anodes with 15 and 40 wt % Si (with thicknesses of 40 and 22 μm, respectively) were prepared with the same Si areal loading, which demonstrates that the lower effective gravimetric capacity of a low Si-content fiber mat anode can be offset by utilizing a thicker electrode.

Whereas previously reported Si anodes prepared by electrospinning followed by fiber pyrolysis have low material loadings and mat densities that limit their use in practical devices, particle/polymer electrospinning can be used to prepare thick, densely packed, yet sufficiently porous, fiber mats with high loadings for high areal and volumetric capacities. A compacted + welded nanofiber mat containing 40 wt % Si and a material loading of 3.49 mg cm^{-2} exhibited areal and volumetric capacities of 4.5 mA h cm^{-2} and 750 mA h cm^{-3}, respectively, at 0.1 C. Furthermore, although most papers in the literature have focused exclusively on characterizing electrodes in half cells, Li–ion battery full cells were built and tested using a Si/C/PAA fiber mat anode and a LiCoO$_2$/C/PVDF fiber cathode (the latter being discussed thoroughly in a prior publication).[21] The electrospun full cell exhibited a high areal capacity of 2.6 mA h cm^{-2}, high energy density of 270 W h kg^{-1}, and moderate cycling stability with 70 % capacity retention after 10 cycles at 0.1 C.

Overall, the results reported herein demonstrate that particle/polymer electrospinning is a viable and attractive technique for the preparation of high-performance porous electrodes for Li–ion batteries. The composition, thickness, fiber volume fraction, and fiber interconnectivity of electrospun mats can be easily controlled to achieve high gravimetric, areal, and volumetric capacities; this flexibility is unique to electrospun particle/polymer mats and is not possible for other electrode fabrication methods. Furthermore, the tech-

nique is compatible with a wide range of particle/polymer combinations and thus can be used to prepare nanofiber electrodes with new active materials and binders as they are developed.

Experimental Section

Electrospinning inks were prepared by mixing Si nanoparticles (50–70 nm) with carbon black (Vulcan XC-72R, Fuel Cell Store) and poly(acrylic acid) (PAA, $M_v = 450\,000$ g mol^{-1}, Sigma–Aldrich) in n-propanol where the solids content in the inks was 17–18 wt%. Two sources of Si nanoparticles (NanoAmor and US Research Nanomaterials, Inc.) were used in this study, but there was no noticeable difference in the physical or electrochemical properties of Si/C/PAA fiber mats prepared with either set of particles. The ratio of Si/C/PAA in the anodes was fixed at either 40/25/35 or 15/50/35 by weight. Fiber mat anodes were created by electrospinning using a single needle spinneret and a custom-made rotating drum collector as described previously.[20] Fiber mats were spun onto an aluminum foil substrate at the following conditions: i) 0.75 and 1.00 mL h^{-1} solution flow rates for anodes with 15 and 40 wt% Si, respectively, ii) 8 kV bias voltage, iii) 8.0 cm spinneret-to-collector distance, and iv) 20–30% relative humidity (small adjustments in relative humidity were required to maintain batch-to-batch consistency of the fiber structure). Electrospinning was performed in an enclosed chamber in which the relative humidity was adjusted by an electronic controller connected to dry and humid air inlets.

Top-down morphology of the electrospun mats was assessed using scanning electron microscopy (Hitachi S4200 and Zeiss Merlin SEMs).

The structure of the fiber mats was further evaluated by X-ray diffraction (XRD, Scintag XDS2000) and energy-dispersive X-ray spectroscopy (EDX, Hitachi TM3030Plus)

Several types of anodes were prepared with 40 wt% Si. The first was an as-spun mat with a fiber volume fraction of ≈ 0.30. The others were compacted and/or welded mats, which were prepared by: i) mechanically compacting an as-spun mat on a hydraulic press at 90 MPa for 40 s at RT to increase the fiber volume fraction and/or ii) exposing the mat to methanol vapor for 1 h at RT to weld the interfiber contacts. Methanol is a solvent for PAA, and thus exposing the Si/C/PAA fiber mats to methanol vapor softened the PAA, causing individual fiber crossings to fuse without disrupting the interfiber void space. For anodes prepared with 15 wt% Si, only a compacted + welded fiber mat was tested. The fiber volume fraction of all compacted mats was 0.80 ± 0.05 as determined by analysis of top-down SEM images of fiber mats using ImageJ as described previously.[20–21]

CR2032 half cells were constructed in an argon-filled glovebox using a free-standing electrospun fiber mat (circular disks 10 mm in diameter, dried overnight at 70 °C under vacuum) as the working electrode and a Li metal counter/reference electrode. The electrolyte was 1.2 M LiPF$_6$ in a mixture of ethylene carbonate and diethyl carbonate (3/7 by volume, BASF Corp.). 30 wt% fluoroethylene carbonate (BASF Corp.) was added to the electrolyte to ensure formation of a stable SEI layer as has been reported in various studies on Si-based anodes.[39,40,58] Two sheets of Celgard 2500 soaked in electrolyte were used as a membrane separator to prevent short circuiting of the cell during crimping, and several additional drops of electrolyte were added to completely fill the cell volume. Cells were crimped at 1000 psi and rested overnight before electrochemical characterization. Galvanostatic charge/discharge experiments were conducted by polarizing the cells between 0.015–1.5 V vs. Li/Li$^+$ at 0.1–1 C on an 8-channel battery tester (5 V/1 mA, MTI Corp.). C-rates for the half cells were calculated assuming a theoretical capacity of 3600 mA h g^{-1} for Si and 372 mA h g^{-1} for carbon. Except otherwise indicated, half-cell capacities are normalized with respect to the entire composite anode (i.e., total amounts of Si, C, and PAA).

Selected half cells were disassembled after cycling, and the anodes were rinsed using dimethyl carbonate before conducting post-mortem analyses. Cross-sectional SEM images of pristine (i.e., uncycled) and cycled fiber mat anodes were collected using a Zeiss Merlin VP microscope (Carl Zeiss Microscopy GmbH, Oberkochen, Germany). The cross-sectional investigations using both SEM and Raman were performed on electrodes broken into halves after freezing them in liquid nitrogen. Raman spectra of pristine and cycled fiber mat anodes were acquired using an Alpha 300 confocal Raman microscope (WITec, GmbH) with a solid-state 532 nm excitation laser, 100× objective, and a grating with 600 grooves mm^{-1}. Raman maps with a spatial resolution on the order of 1 μm and a pixel density of 9 pixels μm^{-2} were collected with an integration time of 2 s per spectrum. The laser power was attenuated to 1 mW for analysis of the pristine electrode. The laser power was further reduced to 100 μW for analysis of the cycled sample to prevent crystallization of the amorphous silicon from laser-induced heating. Raman maps were analyzed using WITec Project Plus software.

A CR2032 full cell containing an electrospun Si/C/PAA anode and an electrospun LiCoO$_2$/C/PVDF cathode was assembled and tested. The LiCoO$_2$/C/PVDF fiber mat cathode was prepared using the ink formulation and electrospinning procedure described in Ref. [28]. The full cell contained the same electrolyte and separator as used in the half cells. To minimize the irreversible capacity loss in the full cell, the Si/C/PAA anode and LiCoO$_2$/C/PVDF cathode were preconditioned in half cells for at least 10 cycles at 0.1 C, as was done in other studies.[21,59–68] The anode/cathode mass ratio in the full cell was 1/13 to ensure good capacity matching of the electrodes (anode/cathode capacity ratio was 0.89). The full cell was characterized using galvanostatic charge/discharge cycling between 2.50–4.20 V at 0.1 C, where the C-rate was calculated based on the measured capacity of the cathode. Full cell capacities were normalized with respect to both electrodes (i.e., the combined amounts of the Si/C/PAA anode and LiCoO$_2$/C/PVDF cathode).

Conflict of interest

The authors declare no conflict of interest.

[1] M. Armand, J.-M. Tarascon, *Nature* **2008**, *451*, 652–657.

[2] J.-M. Tarascon, M. Armand, *Nature* **2001**, *414*, 359–367.

[3] J. B. Goodenough, Y. Kim, *Chem. Mater.* **2010**, *22*, 587–603.

[4] J. B. Goodenough, *Acc. Chem. Res.* **2013**, *46*, 1053–1061.

[5] R. P. Maloney, H. J. Kim, J. S. Sakamoto, *ACS Appl. Mater. Interfaces* **2012**, *4*, 2318–2321.

[6] U. Kasavajjula, C. Wang, A. J. Appleby, *J. Power Sources* **2007**, *163*, 1003–1039.

[7] N. Nitta, G. Yushin, *Part. Part. Syst. Charact.* **2014**, *31*, 317–336.

[8] H. Wu, Y. Cui, *Nano Today* **2012**, *7*, 414–429.

[9] J. Li, N. J. Dudney, J. Nanda, C. Liang, *ACS Appl. Mater. Interfaces* **2014**, *6*, 10083–10088.

[10] A. Mukhopadhyay, B. W. Sheldon, *Prog. Mater. Sci.* **2014**, *63*, 58–116.

[11] A. Tokranov, B. W. Sheldon, C. Li, S. Minne, X. Xiao, *ACS Appl. Mater. Interfaces* **2014**, *6*, 6672–6686.

[12] R. C. de Guzman, J. Yang, M. M.-C. Cheng, S. O. Salley, K. Y. S. Ng, *J. Mater. Sci.* **2013**, *48*, 4823–4833.

[13] L. Hu, H. Wu, S. S. Hong, L. Cui, J. R. McDonough, S. Bohy, Y. Cui, *Chem. Commun.* **2011**, *47*, 367–369.

[14] N. Liu, H. Wu, M. T. McDowell, Y. Yao, C. Wang, Y. Cui, *Nano Lett.* **2012**, *12*, 3315–3321.

[15] C. K. Chan, H. Peng, G. Liu, K. McIlwrath, X. F. Zhang, R. A. Huggins, Y. Cui, *Nat. Nanotechnol.* **2008**, *3*, 31–35.

[16] C. K. Chan, R. N. Patel, M. J. O'Connell, B. A. Korgel, Y. Cui, *ACS Nano* **2010**, *4*, 1443–1450.

[17] N. Liu, L. Hu, M. T. McDowell, A. Jackson, Y. Cui, *ACS Nano* **2011**, *5*, 6487–6493.

[18] H. Zhou, J. Nanda, S. K. Martha, R. R. Unocic, H. M. Meyer 3rd, Y. Sahoo, P. Miskiewicz, T. F. Albrecht, *ACS Appl. Mater. Interfaces* **2014**, *6*, 7607–7614.

[19] E. C. Self, R. Wycisk, P. N. Pintauro, *J. Power Sources* **2015**, *282*, 187–193.

[20] E. C. Self, E. C. McRen, P. N. Pintauro, *ChemSusChem* **2016**, *9*, 208–215.

[21] E. C. Self, E. C. McRen, R. Wycisk, P. N. Pintauro, *Electrochim. Acta* **2016**, *214*, 139–146.

[22] H. G. Wang, D. L. Ma, Y. Huang, X. B. Zhang, *Chem. Eur. J.* **2012**, *18*, 8987–8993.

[23] H. Wang, D. Ma, X. Huang, Y. Huang, X. Zhang, *Sci. Rep.* **2012**, *2*, 701.

[24] L. Zhang, X. Zhang, Z. Wang, J. Xu, D. Xu, L. Wang, *Chem. Commun.* **2012**, *48*, 7598–7600.

[25] Y.-B. Yin, J.-J. Xu, Q.-C. Liu, X.-B. Zhang, *Adv. Mater.* **2016**, *28*, 7494–7500.

[26] S. Yuan, Y.-H. Zhu, W. Li, S. Wang, D. Xu, L. Li, Y. Zhang, X.-B. Zhang, *Adv. Mater.* **2017**, *29*, 1602469.

[27] K. Fu, L. Xue, O. Yildiz, S. Li, H. Lee, Y. Li, G. Xu, L. Zhou, P. D. Bradford, X. Zhang, *Nano Energy* **2013**, *2*, 976–986.

[28] Y. Liu, K. Huang, Y. Fan, Q. Zhang, F. Sun, T. Gao, Z. Wang, J. Zhong, *Electrochim. Acta* **2013**, *102*, 246–251.

[29] L. Ji, X. Zhang, *Energy Environ. Sci.* **2010**, *3*, 124.

[30] L. Xue, K. Fu, Y. Li, G. Xu, Y. Lu, S. Zhang, O. Toprakci, X. Zhang, *Nano Energy* **2013**, *2*, 361–367.

[31] Y. Xu, Y. Zhu, F. Han, C. Luo, C. Wang, *Adv. Energy Mater.* **2015**, *5*, 1400753.

[32] Z. Favors, H. H. Bay, Z. Mutlu, K. Ahmed, R. Ionescu, R. Ye, M. Ozkan, C. S. Ozkan, *Sci. Rep.* **2015**, *5*, 8246.

[33] H. Wu, G. Zheng, N. Liu, T. J. Carney, Y. Yang, Y. Cui, *Nano Lett.* **2012**, *12*, 904–909.

[34] X. Zhang, L. Ji, O. Toprakci, Y. Liang, M. Alcoutlabi, *Polym. Rev.* **2011**, *51*, 239–264.

[35] L. Liu, J. Lyu, T. Li, T. Zhao, *Nanoscale* **2016**, *8*, 701–722.

[36] H.-G. Wang, S. Yuan, D.-L. Ma, X.-B. Zhang, J.-M. Yan, *Energy Environ. Sci.* **2015**, *8*, 1660–1681.

[37] O. Rios, S. K. Martha, M. A. McGuire, W. Tenhaeff, K. More, C. Daniel, J. Nanda, *Energy Technol.* **2014**, *2*, 773-777.

[38] Q. Xiao, Q. Zhang, Y. Fan, X. Wang, R. A. Susantyoko, *Energy Environ. Sci.* **2014**, *7*, 2261.

[39] G. Liu, S. Xun, N. Vukmirovic, X. Song, P. Olalde-Velasco, H. Zheng, V. S. Battaglia, L. Wang, W. Yang, *Adv. Mater.* **2011**, *23*, 4679–4683.

[40] S. J. Park, H. Zhao, G. Ai, C. Wang, X. Song, N. Yuca, V. S. Battaglia, W. Yang, G. Liu, *J. Am. Chem. Soc.* **2015**, *137*, 2565–2571.

[41] H. Zhao, Z. Wang, P. Lu, M. Jiang, F. Shi, X. Song, Z. Zheng, X. Zhou, Y. Fu, G. Abdelbast, X. Xiao, Z. Liu, V. S. Battaglia, K. Zaghib, G. Liu, *Nano Lett.* **2014**, *14*, 6704–6710.

[42] M. Wu, X. Song, X. Liu, V. Battaglia, W. Yang, G. Liu, *J. Mater. Chem. A* **2015**, *3*, 3651–3658.

[43] A. Magasinski, B. Zdyrko, I. Kovalenko, B. Hertzberg, R. Burtovyy, C. F. Huebner, T. F. Fuller, I. Luzinov, G. Yushin, *ACS Appl. Mater. Interfaces* **2010**, *2*, 3004–3010.

[44] J. S. Bridel, T. Azais, M. Morcrette, J. M. Tarascon, D. Larcher, *Chem. Mater.* **2010**, *22*, 1229–1241.

[45] I. Kovalenko, B. Zdyrko, A. Magasinski, B. Hertzberg, Z. Milicev, R. Burtovyy, I. Luzinov, G. Yushin, *Science* **2011**, *334*, 75–79.

[46] Z. Li, J. T. Zhang, Y. M. Chen, J. Li, X. W. Lou, *Nat. Commun.* **2015**, *6*, 8850.

[47] T. Liu, Q. C. Liu, J. J. Xu, X. B. Zhang, *Small* **2016**, *12*, 3101–3105.

[48] T. Xu, H. Zhang, H. Zhong, Y. Ma, H. Jin, Y. Zhang, *J. Power Sources* **2010**, *195*, 8075–8079.

[49] H. Buqa, D. Goers, M. Holzapfel, M. E. Spahr, P. Novák, *J. Electrochem. Soc.* **2005**, *152*, A474.

[50] J. B. Dunn, L. Gaines, J. Barnes, J. Sullivan, M. Wang, *Argonne National Laboratory Report ANL/ESD/12-3*, **2012** https://greet.es.anl.gov/publication-lib-lca.

[51] M. Shimizu, H. Usui, T. Suzumura, H. Sakaguchi, *J. Phys. Chem. C* **2015**, *119*, 2975–2982.

[52] J. Nanda, M. K. Datta, J. T. Remillard, A. O'Neill, P. N. Kumta, *Electrochem. Commun.* **2009**, *11*, 235–237.

[53] R. C. Teixeira, I. Doi, M. B. P. Zakia, J. A. Diniz, J. W. Swart, *Mater. Sci. Eng. B* **2004**, *112*, 160–164.

[54] E. Pollak, G. Salitra, V. Baranchugov, D. Aurbach, *J. Phys. Chem. C* **2007**, *111*, 11437–11444.

[55] D. M. Piper, J. J. Travis, M. Young, S. B. Son, S. C. Kim, K. H. Oh, S. M. George, C. Ban, S. H. Lee, *Adv. Mater.* **2014**, *26*, 1596–1601.

[56] V. Aravindan, J. Sundaramurthy, P. S. Kumar, N. Shubha, W. C. Ling, S. Ramakrishna, S. Madhavi, *Nanoscale* **2013**, *5*, 10636–10645.

[57] S. Jayaraman, V. Aravindan, P. Suresh Kumar, W. Chui Ling, S. Ramakrishna, S. Madhavi, *ACS Appl. Mater. Interfaces* **2014**, *6*, 8660–8666.

[58] S. Xun, B. Xiang, A. Minor, V. Battaglia, G. Liu, *J. Electrochem. Soc.* **2013**, *160*, A1380–A1383.

[59] F. Bonino, S. Brutti, P. Reale, B. Scrosati, L. Gherghel, J. Wu, K. Müllen, *Adv. Mater.* **2005**, *17*, 743–746.

[60] A. Caballero, L. Hernan, J. Morales, *ChemSusChem* **2011**, *4*, 658–663.

[61] I. R. M. Kottegoda, Y. Kadoma, H. Ikuta, Y. Uchimoto, M. Wakihara, *J. Electrochem. Soc.* **2005**, *152*, A1595.

[62] Ó. Vargas, Á. Caballero, J. Morales, *Electrochim. Acta* **2015**, *165*, 365–371.

[63] C. Chae, H. Park, D. Kim, J. Kim, E.-S. Oh, J. K. Lee, *J. Power Sources* **2013**, *244*, 214–221.

[64] J. Hassoun, F. Croce, I. Hong, B. Scrosati, *Electrochem. Commun.* **2011**, *13*, 228–231.

[65] R. Kataoka, T. Mukai, A. Yoshizawa, T. Sakai, *J. Electrochem. Soc.* **2013**, *160*, A1684–A1689.

[66] K.-L. Lee, J.-Y. Jung, S.-W. Lee, H.-S. Moon, J.-W. Park, *J. Power Sources* **2004**, *130*, 241–246.

[67] R. Verrelli, J. Hassoun, A. Farkas, T. Jacob, B. Scrosati, *J. Mater. Chem. A* **2013**, *1*, 15329.

[68] Y. Wang, Y. Wang, D. Jia, Z. Peng, Y. Xia, G. Zheng, *Nano Lett.* **2014**, *14*, 1080–1084.